A Domain Decomposition Based ALE Framework for Three-dimensional Fluid-structure Interaction with Application in Blood Flow Computation

Yuqi Wu[a], Xiao-Chuan Cai[b]

[a]*Department of Applied Mathematics, University of Colorado at Boulder, Boulder, CO, 80309*
[b]*Department of Computer Science, University of Colorado at Boulder, Boulder, CO, 80309*

Abstract

In this paper, we introduce and study a parallel scalable domain decomposition method for the simulation of blood flows in three-dimensional compliant arteries, by using a fully coupled system of linear elasticity equation and incompressible Navier-Stokes equations in an arbitrary Lagrangian-Eulerian framework. The system is discretized with a fully-implicit finite element method on unstructured moving meshes and solved by a Newton-Krylov algorithm preconditioned with an overlapping additive Schwarz method. The investigation focuses on the accuracy and parallel scalability of the algorithm. Simulations based on the patient-specific pulmonary artery geometries are performed on a supercomputer with thousands of processors. Our algorithm is shown to be scalable with a large number of processors and for problems with millions of unknowns.

Keywords: fluid-structure interaction, blood flow simulation, restricted additive Schwarz, domain decomposition, parallel computing

1. Introduction

Computer modeling of blood flow in the arteries is an important and very challenging problem. Such simulations in the virtual environment have been used to study the vascular system in a variety of applications including predicting the development of artery diseases and the treatment for the diseases [7, 19]. In order to understand, computationally, the sophisticated hemodynamics in the arteries, it is essential to take into account the deformability of the artery walls. Simulations with the rigid wall assumption preclude the ability to predict the pressure wave propagation phenomena, which is the crucial characteristics of the blood flow. In the fluid-structure interaction (FSI) problems, different approaches are used to keep track of the fluid-structure coupling on the interface, e.g. the arbitrary Lagrangian-Eulerian (ALE) framework [16, 17], the space-time formulation [4, 22] and the coupled momentum method [12]. In our approach, we describe the fluid equations within the ALE framework by introducing a new equation for the fluid domain motion, ensuring that the fluid-structure coupling conditions are satisfied exactly on the interface. Although the computation of the fluid domain motion can be avoided in the coupled momentum method, the ALE formulation is not limited to small wall deformations, which is a prerequisite in the coupled momentum method [12].

Another challenging issue arise in the numerical computation of the coupled system is the coupling formulation between the fluid and solid subsystems. Two well-known formulations are iterative and monolithic. In iterative approaches, the fluid and the structure equations are solved one after the other repeatedly, until some desired tolerance is reached [9, 13]. The convergence of these approaches is difficult to achieve in some situations [6], since the approaches are very similar to nonlinear Gauss-Seidel with two large blocks. In contrast, we develop a monolithic coupling as in [2, 8], where the fluid, the structure and the mesh

Email addresses: yuqi.wu@colorado.edu (Yuqi Wu), cai@cs.colorado.edu (Xiao-Chuan Cai)

movement equations are solved simultaneously in a fully coupled fashion and the coupling conditions are enforced strongly as part of the system. The monolithic approach has been shown to be more robust. Many of the convergence problems encountered within the iterative approaches can be avoided.

However, there is a price to pay in the monolithic approach. Solving the fully-coupled system is computationally more expensive. The equation for the fluid domain motion introduced in the ALE formulation brings in a new field of variables and further nonlinearity. And the monolithic approach requires a fully coupled FSI solver, precluding the use of existing fast fluid and structure solver. Furthermore, the blood flow simulations often results in a very large scale computation, making the use of massively parallel computer a must. It necessitates the development of a fully coupled FSI solver that is not only robust with respect to the physical variables such as Reynolds number, Poisson ratio, etc, but also highly scalable on machines with a large number of processors. In this paper, we focus on developing a class of parallel scalable Newton-Krylov-Schwarz method with an overlapping restricted additive Schwarz preconditioner for solving the fully coupled FSI system in 3D, with emphasis on the robustness and the parallel scalability of the algorithms.

The rest of the paper is organized as follows. In Section 2, we describe the formulation of the FSI problem, and also the discretization of the problem, both in space and time. In Section 3, we present the Newton-Krylov-Schwarz method for solving the nonlinear fully coupled system. In Section 4, we demonstrate the effectiveness of the algorithm by showing some numerical results using different geometries and problem sizes, and report the parallel performance of the algorithm. Finally, we offer some concluding remarks in Section 5.

2. Mathematical formulation and discretization

Our fully coupled approach is described by a system with three components, the linear elasticity equation for the wall structure in the Lagrangian frame of reference, the incompressible Navier-Stokes equations for the fluid in the ALE framework, and the Laplace equation for the displacement of the fluid domain. Let $\Omega_s \in R^3$ be the structure domain. The displacement $\mathbf{x}_s$ of the artery walls is assumed to satisfy

$$\rho_s \frac{\partial^2 \mathbf{x}_s}{\partial t^2} + \alpha \frac{\partial \mathbf{x}_s}{\partial t} - \nabla \cdot \sigma_s = \mathbf{f}_s \quad \text{in } \Omega_s, \tag{1}$$

where ρ_s is the density of the structure, and $\sigma_s = \lambda_s(\nabla \cdot \mathbf{x}_s)I + \mu_s(\nabla \mathbf{x}_s + \nabla \mathbf{x_s}^T)$ is the Cauchy stress tensor. The Lamé parameters λ_s and μ_s are related to the Young's modulus E and the Poisson ratio ν_s by $\lambda_s = \nu_s E/((1+\nu_s)(1-2\nu_s))$ and $\mu_s = E/(2(1+\nu_s))$. As in [18, 21], the mass-proportional damping coefficient α is considered in our formulation to represent the damping effect of the surrounding tissue on the structure. Other choice concerning the surrounding tissue effects by imposing particular boundary condition on the external artery walls can be found in [8].

To model the fluid in a moving domain $\Omega_f(t) \in R^3$, the displacement of the fluid domain $\mathbf{x}_f$ in the reference configuration $\Omega_0 \in R^3$ is assumed to satisfy a Laplace equation,

$$\Delta \mathbf{x}_f = 0 \quad \text{in } \Omega_0.$$

We define an ALE mapping A_t from Ω_0 to $\Omega_f(t)$:

$$A_t : \Omega_0 \to \Omega_f(t), \quad A_t(\mathbf{Y}) = Y + \mathbf{x_f}(Y), \quad \forall \mathbf{Y} \in \Omega_0,$$

where $\mathbf{Y}$ is referred to as the ALE coordinates. The incompressible Navier-Stokes equations defined on the moving domain $\Omega_f(t)$ are written in the ALE form as

$$\rho_f \left.\frac{\partial \mathbf{u}_f}{\partial t}\right|_Y + \rho_f[(\mathbf{u}_f - \omega_g)\cdot\nabla]\mathbf{u}_f - \nabla \cdot \sigma_f = 0 \quad \text{in } \Omega_f(t),$$
$$\nabla \cdot \mathbf{u}_f = 0 \quad \text{in } \Omega_f(t),$$

where ρ_f is the fluid density, $\mathbf{u}_f$ is the fluid velocity, and $\sigma_f = -p_f I + \mu_f(\nabla \mathbf{u_f} + \nabla \mathbf{u_f}^T)$ is the Cauchy stress tensor. $\omega_g = \partial \mathbf{x_f}/\partial t$ is the velocity of the moving domain and Y indicates that the time derivative is taken

with respect to the ALE coordinates. On the inlet boundary Γ_i, a given velocity profile is prescribed. On the outlet boundary Γ_o, the zero traction condition $\sigma_f \cdot \mathbf{n} = 0$ is considered, where $\mathbf{n}$ is the unit outward normal. These boundary conditions may be chosen differently, depending on the problem at hand.

More importantly, three coupling conditions are strongly enforced on the fluid-structure interface Γ_w

$$\sigma_s \cdot \mathbf{n}_s = -\sigma_f \cdot \mathbf{n}_f, \quad \mathbf{u_f} = \frac{\partial \mathbf{x_s}}{\partial t}, \quad \mathbf{x}_f = \mathbf{x}_s, \tag{2}$$

where $\mathbf{n}_s$, $\mathbf{n}_f$ are unit normal vectors on the fluid-structure interface.

By introducing the structure velocity $\dot{\mathbf{x}}_\mathbf{s}$ as an additional unknown variable, we can rewrite the structure momentum equation (1) as a first-order system of equations. We define the variational space of the structure problem as

$$X = \left\{ \mathbf{x_s} \in [H^1(\Omega_s)]^3 : \mathbf{x_s} = 0 \text{ on } \Gamma_s \right\}.$$

The weak form of the structure subproblem is stated as follows: Find $\mathbf{x_s} \in X$ and $\dot{\mathbf{x}}_\mathbf{s} \in X$ such that $\forall \phi_s \in X$ and $\forall \varphi_s \in X$,

$$\begin{aligned} B_s(\{\mathbf{x_s}, \dot{\mathbf{x}}_\mathbf{s}\}, \{\phi_s, \varphi_s\}; \sigma_f) = \rho_s \frac{\partial}{\partial t} \int_{\Omega_s} \dot{\mathbf{x}}_\mathbf{s} \cdot \phi_s \, d\Omega + \alpha \int_{\Omega_s} \frac{\partial \mathbf{x_s}}{\partial t} \cdot \phi_s \, d\Omega + \int_{\Omega_s} \nabla \phi_s : \sigma_s \, d\Omega \\ - \int_{\Gamma_w} \phi_s \cdot (\sigma_f \cdot \mathbf{n}_s) \, ds - \int_{\Omega_s} \mathbf{f}_s \cdot \phi_s \, d\Omega + \int_{\Omega_s} \left(\frac{\partial \mathbf{x_s}}{\partial t} - \dot{\mathbf{x}}_\mathbf{s} \right) \cdot \varphi_s \, d\Omega = 0. \end{aligned}$$

The variational spaces of the fluid subproblem are time dependent, and the solution of the structure subproblem provides an essential boundary condition for the fluid subproblem by (2). We define the trial and weighting function spaces as:

$$\begin{aligned} V &= \left\{ \mathbf{u}_f \in [H^1(\Omega_f(t))]^3 : \mathbf{u}_f = g \text{ on } \Gamma_i, \mathbf{u}_f = \partial \mathbf{x}_s / \partial t \text{ on } \Gamma_w \right\}, \\ V_0 &= \left\{ \mathbf{u}_f \in [H^1(\Omega_f(t))]^3 : \mathbf{u}_f = 0 \text{ on } \Gamma_i \cup \Gamma_w \right\}, \\ P &= L^2\left(\Omega_f(t)\right). \end{aligned}$$

The weak form of the fluid problem reads: Find $\mathbf{u}_f \in V$ and $p_f \in P$ such that $\forall \phi_f \in V_0$ and $\forall \psi_f \in P$,

$$\begin{aligned} B_f(\{\mathbf{u}_f, p_f\}, \{\phi_f, \psi_f\}; \mathbf{x}_f) = \rho_f \int_{\Omega_f(t)} \left. \frac{\partial \mathbf{u}_f}{\partial t} \right|_Y \cdot \phi_f \, d\Omega + \rho_f \int_{\Omega_f(t)} \left[(\mathbf{u}_f - \omega_g) \cdot \nabla \right] \mathbf{u}_f \cdot \phi_f \, d\Omega \\ - \int_{\Omega_f(t)} p_f (\nabla \cdot \phi_f) \, d\Omega + 2\mu_f \int_{\Omega_f(t)} \epsilon(\mathbf{u}_f) : \epsilon(\phi_f) \, d\Omega + \int_{\Omega_f(t)} (\nabla \cdot \mathbf{u}_f) \psi_f \, d\Omega = 0, \end{aligned}$$

where $\epsilon(\mathbf{u}_f) = (\nabla \mathbf{u}_f + \nabla \mathbf{u}_f^T)/2$. The weak form of the domain movement problem reads: Find $\mathbf{x}_f \in Z$ such that $\forall \xi \in Z_0$,

$$B_m(\mathbf{x}_f, \xi) = \int_{\Omega_0} \nabla \xi : \nabla \mathbf{x}_f \, d\Omega = 0.$$

And the variational spaces are defined as

$$\begin{aligned} Z_0 &= \{ \mathbf{x}_f \in [H^1(\Omega_0)]^3 : \mathbf{x}_f = 0 \text{ on } \Gamma_i \cup \Gamma_o \cup \Gamma_w \}, \\ Z &= \{ \mathbf{x}_f \in [H^1(\Omega_0)]^3 : \mathbf{x}_f = \mathbf{x}_s \text{ on } \Gamma_w, \mathbf{x}_f = 0 \text{ on } \Gamma_i \cup \Gamma_o \}. \end{aligned}$$

We discretize the fully coupled problem in space with a finite element method, consisting of unstructured P1-P1 stabilized elements for the fluid, P1 elements for the structure and P1 elements for the fluid domain motion. We denote the finite element subspaces X_h, V_h, $V_{h,0}$, P_h, Z_h, $Z_{h,0}$ as the counterparts of their infinite dimensional subspaces. Because the fluid problem requires that the pair V_h and P_h satisfy the LBB inf-sup condition, additional stabilization terms are needed in the formulation with equal-order interpolation of the

velocity and the pressure as described in [20, 24]. The semi-discrete stabilized finite element formulation for the fluid problem reads as follows: Find $\mathbf{u}_f \in V_h$ and $p_f \in P_h$, such that $\forall \phi_f \in V_{h,0}$ and $\forall \psi_f \in P_h$,

$$B\left(\{\mathbf{u}_f, p_f\}, \{\phi_f, \psi_f\}; \mathbf{x}_f\right) = 0,$$

with

$$\begin{aligned} B\left(\{\mathbf{u}_f, p_f\}, \{\phi_f, \psi_f\}; \mathbf{x}_f\right) = B_f\left(\{\mathbf{u}_f, p_f\}, \{\phi_f, \psi_f\}; \mathbf{x}_f\right) &+ \sum_{K \in \mathcal{T}_f^h} \left(\nabla \cdot \mathbf{u}_f, \tau_c \nabla \cdot \phi_f\right)_K \\ &+ \sum_{K \in \mathcal{T}_f^h} \left(\left.\frac{\partial \mathbf{u}_f}{\partial t}\right|_Y + (\mathbf{u}_f - \omega_g) \cdot \nabla \mathbf{u}_f + \nabla p_f, \tau_m \left((\mathbf{u}_f - \omega_g) \cdot \nabla \phi_f + \nabla \psi_f\right) \right)_K \\ &+ \sum_{K \in \mathcal{T}_f^h} \left(\overline{\mathbf{u}}_\mathbf{f} \cdot \nabla \mathbf{u}_f, \phi_f\right)_K + \sum_{K \in \mathcal{T}_f^h} \left(\overline{\mathbf{u}}_\mathbf{f} \cdot \nabla \mathbf{u}_f, \tau_b \overline{\mathbf{u}}_\mathbf{f} \cdot \nabla \phi_f\right)_K, \end{aligned}$$

where $\mathcal{T}_f^h = \{K\}$ is the given unstructured tetrahedral fluid mesh, and $\overline{\mathbf{u}}_\mathbf{f}$ is the conservation-restoring advective velocity introduced in [20],

$$\overline{\mathbf{u}}_\mathbf{f} = -\tau_m \left(\left.\frac{\partial \mathbf{u}_f}{\partial t}\right|_Y + (\mathbf{u}_f - \omega_g) \cdot \nabla \mathbf{u}_f + \nabla p_f \right).$$

Here τ_c, τ_m and τ_b are stabilization parameters as discussed in [23].

We form the finite dimensional fully coupled FSI problem as follows: Find $x_s \in X_h$, $\dot{x}_s \in X_h$, $u_f \in V_h$, $p_f \in P_h$ and $x_f \in Z_h$ such that $\forall \phi_s \in X_h$, $\forall \varphi_s \in X_h$, $\forall \phi_f \in V_{h,0}$, $\forall \psi_f \in P_h$, and $\forall \xi \in Z_{h,0}$,

$$B_s(\{x_s, \dot{x}_s\}, \{\phi_s, \varphi_s\}; \sigma_f) + B(\{u_f, p_f\}, \{\phi_f, \psi_f\}; x_f) + B_m(x_f, \xi) = 0. \tag{3}$$

The system (3) is further discretized in time with a backward Euler scheme. Since the temporal discretization scheme is fully implicit, at each time step, we obtain the solution x^n at the n^{th} time step from the previous time step by solving a sparse, nonlinear algebraic system

$$\mathcal{F}_n(x^n) = 0, \tag{4}$$

where x^n corresponds to the nodal values of the fluid velocity $\mathbf{u}_f$, the fluid pressure p_f, the fluid mesh displacement $\mathbf{x}_f$, the structure displacement $\mathbf{x}_s$ and the structure velocity $\dot{\mathbf{x}}_s$ at the n^{th} time step. For simplicity, we ignore the script n for the rest of the paper.

3. A highly scalable nonlinear solver

To design an algorithm for (4) that is highly scalable in terms of the total compute time, many important factors need to be taken into consideration. None of the components of the algorithm is new, but to arrive at the best combination, we have to consider not only the properties of the nonlinear system, the properties of the domain decomposition methods, but also the software and hardware of our computational environment. In the Newton-Krylov-Schwarz approach, the nonlinear system (4) is solved via the inexact Newton method [10]. At each Newton step the new solution $x^{(k+1)}$ is obtained from the current solution $x^{(k)}$ by $x^{(k+1)} = x^{(k)} + \theta^{(k)} s^{(k)}$, where the step length $\theta^{(k)}$ is determined by a cubic line search technique. The Newton correction $s^{(k)}$ is approximated by solving a preconditioned Jacobian system $J_k M_k^{-1} M_k s^{(k)} = -\mathcal{F}(x^{(k)})$ with GMRES, where M_k^{-1} is a one-level restricted additive Schwarz preconditioner [5].

The evaluation of the Jacobians of the fully coupled system is non-trivial. The difficulty lies in the evaluation of the cross derivatives, e.g. the derivatives of fully coupled system with respect to the mesh movement. One solution is to use the finite difference approximation to calculate the cross derivatives [15], but such approximation is required at each Newton iteration and is computationally expensive. Another solution is

to use a computationally cheap approximation [14], but this often deteriorates the overall convergence. In our implementation, we compute the Jacobians analytically including all those cross derivatives.

To define the domain decomposition preconditioner, we first partition the finite element mesh (which consists of the meshes for all components of the coupled system) into non-overlapping subdomains Ω_ℓ^h, $\ell = 1, \ldots, N$, where the number of subdomain N is always the same as the number of processors np. Then, each subdomain Ω_ℓ^h is extended to an overlapping subdomain $\Omega_\ell^{h,\delta}$. Here δ is an integer indicating the level of overlap. Note that the decomposition of the mesh is completely independent of which physical variables are defined for a given mesh point. The number of variables at a given mesh point is considered for the purpose of load balancing. The one-level restricted additive Schwarz preconditioner is defined by

$$M_k^{-1} = \sum_{\ell=1}^{N} (R_\ell^0)^T J_\ell^{-1} R_\ell,$$

where R_ℓ^0 and R_ℓ are restrictions to the degrees of freedom in the non-overlapping subdomain Ω_ℓ^h and the overlapping subdomain $\Omega_\ell^{h,\delta}$, respectively. J_ℓ is a restriction of the Jacobian matrix defined by $J_\ell = R_\ell J_k R_\ell^T$. Sparse LU or incomplete LU factorization can be used to obtain the inverse or an approximate inverse of the subdomain Jacobian. To improve the efficiency for the costly LU factorization, we also consider some point-block versions of LU and ILU that keep the coupling between all physical components of each mesh point.

4. Numerical results

In this section, we report some numerical results of the proposed fully coupled FSI solver by simulating the blood flows in compliant arteries. We first validate our solver by testing a benchmark 3D FSI problem. We then investigate the numerical behavior and parallel performance of our solver with two complex branching geometries derived from clinical data. Our solver is implemented using PETSc library [1]. All computations are performed on the Janus supercomputer at the University of Colorado at Boulder.

4.1. A benchmark case

A benchmark 3D FSI problem consists of a straight cylinder representing the fluid domain with length 5 cm and radius 0.5 cm, and the surrounding wall with thickness 0.1 cm. A constant traction $\sigma_f \cdot \mathbf{n} = 1.33 \cdot 10^4$ $dynes/cm^2$ is imposed on the inlet boundary for 3 ms. A zero traction condition is applied to the fluid at the outlet boundary. The fluid is characterized with viscosity $\mu_f = 0.03$ cm^2/s, and density $\rho_f = 1.0$ g/cm^3. The Young's modulus $E = 3 \cdot 10^6$ $g/(cm\ s^2)$, the Poisson ratio $\nu_s = 0.3$, and the structure density $\rho_s = 1.2$ g/cm^3 are the parameters of the structure model. The damping parameter α is set to be zero in this case.

The fluid and the structure are initially at rest and the simulation is run on a mesh with $2.41 \cdot 10^6$ elements and $3.08 \cdot 10^6$ degrees of freedom, for a total time of 10 ms with a time step size $\Delta t = 0.1$ ms. The simulation proceeds to the next time step when the residual of the nonlinear system is less than 10^{-6}. To validate our algorithm, we show the computed fluid pressure and the structure deformation at $t = 2.5$, 5.0, 10.0 ms as in Figure 1. Our results show good agreement with the published results [9, 11]. The pressure wave propagation along the cylinder is observed. The wall structure deforms in response to the propagation of the wall pressure, which is a key feature of the fluid-structure interaction.

4.2. A two-branch artery case

In this subsection, we perform simulations for a branching geometry with two branches obtained from a pulmonary artery. The artery wall thickness is assume to be 10% of the local arterial diameter. For the inlet, we prescribe a pulsatile periodic flow wave, with a period T of 0.6 s. For the outlets, the relation $P = QR$ is implicitly prescribed on the outflow boundaries as the resistance boundary condition, where $Q = \int_\Gamma \mathbf{u}_f \cdot \mathbf{n}\, ds$ represents the flow rate at the outflow boundaries [12, 25]. The resistance $R = 1408.0$ $dyn \cdot s/cm^5$ and $R = 677.6$ $dyn \cdot s/cm^5$ at the left artery outlet and the right artery outlet, respectively. The elastic artery

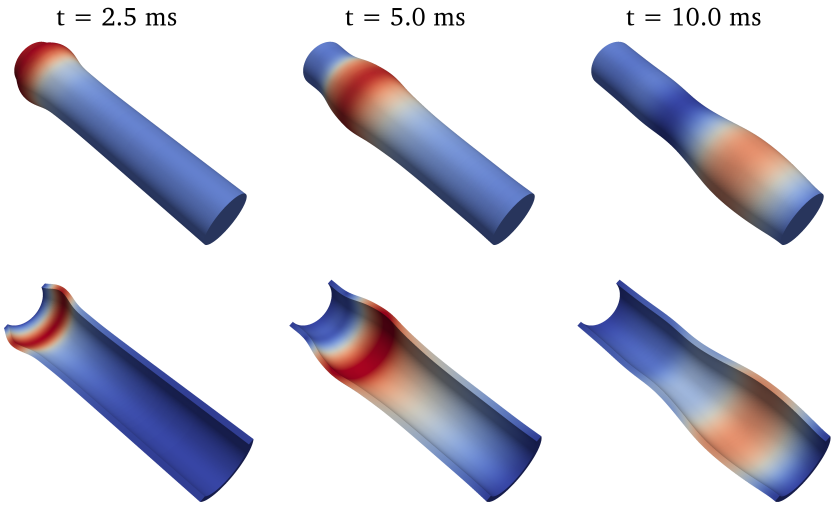

Figure 1: Pressure wave propagation and structure deformation. The deformation is amplified by a factor of 12 for visualization purpose only.

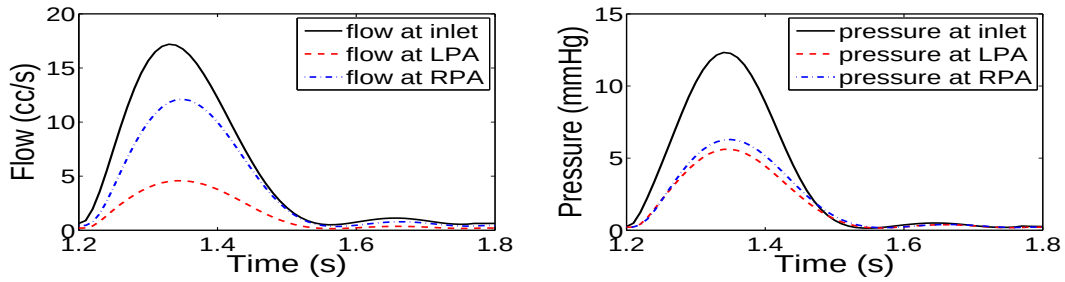

Figure 2: Flow waves and pressure at the inlet and outlets over one cardiac cycle, obtained using the resistance outflow boundary condition. Figure on the left represents the flow rate at the inlet and outlets, and figure on the right shows the fluid pressure at the inlet and outlets.

wall is characterized with density of 1.2 g/cm^3, Young's modulus of 1.5×10^6 $g/(cm\ s^2)$, the Poisson ratio of 0.48, and the damping parameters $\alpha = 6.0 \times 10^3$, which are chosen in the literature [18, 21]. The blood is modeled with a density of 1.0 g/cm^3 and kinematic viscosity of 0.035 cm^2/s. All the physical parameters chosen are physiologically realistic. The simulations are run for 3 cardiac cycles with a time step size of 0.001 s. In Figure 2, we show the simulated results for fluid flow and pressure at the inlet, the left artery outlet (LPA), and the right artery outlet (RPA) during one cardiac cycle. The outflow lags the inflow due to the compliance of the arterial wall. The computed phase shift between the inflow and the outflow at RPA is 0.02 s. Figure 3 shows snapshots of the fluid velocity field at two phases of the cardiac cycle, the peak systole, and early-diastole. The fully three-dimensional flow field is quite complex, especially in the diastole phase. Figure 4 shows the arterial wall velocity vectors at the same two phases, illustrating the corresponding wall movement in response to the fluid dynamics. Such complex flow structures are usually very difficult to be measured clinically, high resolution computer provides a unique way to reveal the phenomena.

We next study the parallel performance and the scalability of our solver to the fully coupled FSI problem. Unless otherwise specified, the stopping criterion for the Newton iteration is when the relative residual norm of the nonlinear system is less than 10^{-6}. The accuracy of preconditioned Jacobian system is governed by the relative tolerance of 10^{-6}. The time step size is fixed as $\Delta t = 0.001\ s$, and the simulation is stopped after 10 time steps. As shown in Figure 5, our algorithm shows satisfactory strong scalability for problem sizes with over 4 million degrees of freedoms and with up to 3072 processors. As we increase the

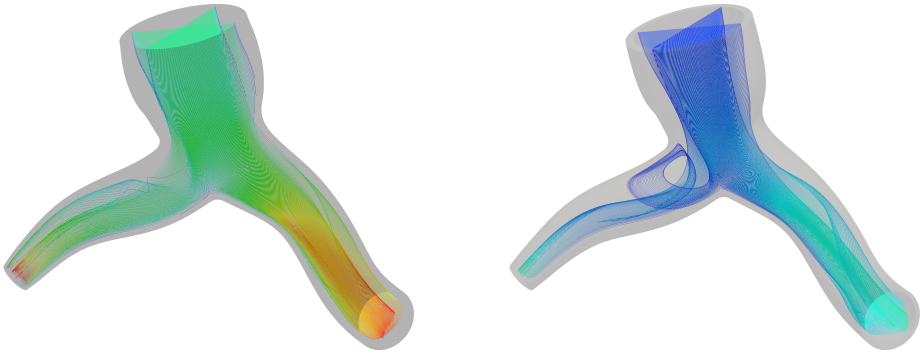

Figure 3: Flow in a pulmonary artery with two branches at the peak systole (left) and the early diastole (right). The fluid streamlines are colored by velocity magnitude.

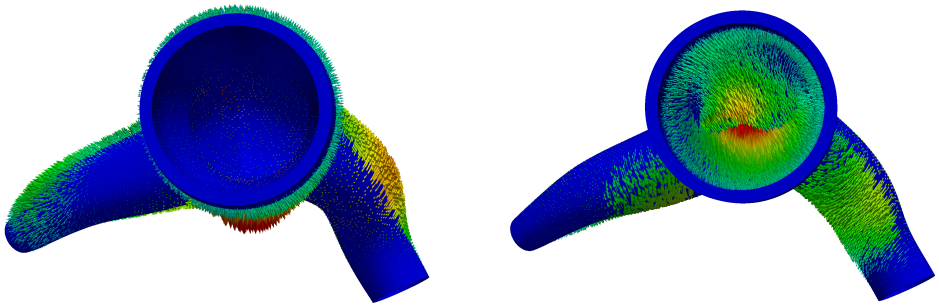

Figure 4: Arterial wall velocity vectors obtained at two points of the cardiac cycle: peak systole (left), early diastole (right).

number of processors, the compute time decreases, and the parallel speedup is nearly ideal. It is worth noting that the growth in GMRES iterations for large processor counts may be a problem if we consider to solve the problem on a much larger mesh and with a larger number processors. In those situations, one possible solution to improve the scalability is the use of a multilevel preconditioner. In our algorithm with an overlapping Schwarz preconditioner, the choice of subdomain solver has a significant impact to the overall performance. In Table 1, we show the results using point-block LU (BLU) and point-block ILU with 2 levels of fill-ins (BILU(2)), by comparing with the results using LU. When LU is used as the subdomain solver, the subdomain problem is solved exactly. We obtain the best performance in terms of GMRES iterations. However, LU factorization is computationally expensive especially when the number of processors is small. Using the point-block factorizations helps improving the efficiency of the factorization. Both of the point-block factorizations shown in the table reduce the fill-in ratio needed in the decomposition. Without deteriorating the convergence, the compute time is reduced by almost 50% if we replace LU by point-block LU. In the case of BILU(2), although there is a mild growth in the number of GMRES iterations, the compute time is further reduced. Comparing with the results using LU factorization, using BILU(2) as the subdomain solve saves nearly 75% of the compute time when the processors is small.

4.3. Complex branching artery case

Here we perform simulations for a larger and more complicated branching geometry obtained from a biplane angiography data from a pulmonary artery. We assume the wall thickness is 10% of the artery radius. The solid density is 1.2 g/cm^3; the Young's modulus of the structure is 7.5×10^5 $g/(cm\ s^2)$; the Poisson ratio is 0.48. The fluid density is 1.0 g/cm^3, and the kinematic viscosity is 0.035 cm^2/s. The inlet

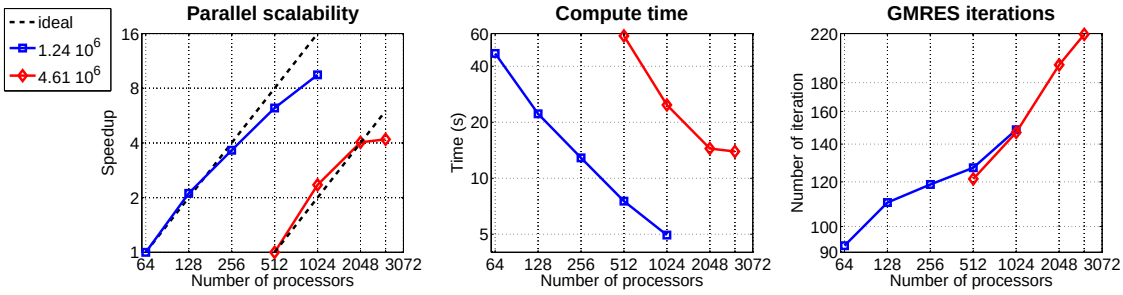

Figure 5: Parallel speedup, average compute time per time step, and average GMRES iterations per Newton iteration for the two branching problem with increasing number of processors. The number of unknowns of each problem is listed in the legend.

	LU				BLU				BILU(2)			
np	NI	GMRES	time	fill-in	NI	GMRES	time	fill-in	NI	GMRES	time	fill-in
128	2.0	62.50	95.38	16.73	2.0	62.50	50.73	14.66	2.0	110.30	22.21	4.76
256	2.0	76.50	35.16	13.23	2.0	76.50	21.92	10.62	2.0	118.75	12.87	4.58
512	2.0	102.25	17.06	8.91	2.0	102.30	9.58	8.91	2.0	127.15	7.53	4.75
1024	2.0	129.45	8.09	6.57	2.0	129.45	6.18	5.10	2.0	148.50	4.94	4.86

Table 1: Performance with respect to the number of processors for different subdomain solvers. The tests are carried on a mesh with $1.24 \cdot 10^6$ unknowns with fixed overlap size $\delta = 1$. "*np*" denotes the number of processors. "NI" denotes the average Newton iteration per time step. "GMRES" denotes the average GMRES iterations per Newton step. "time" refers to the average compute time, in seconds, per time step. "fill-in" refers to the average fill-in needed in the factorization per iteration.

boundary condition is parabolic in space and time profile like $1+\sin(\pi t)$ with a maximum of 16.5 cm/s. The zero-traction boundary conditions are imposed at the outflows. Since the purpose of these simulations is mainly to test the performance of our algorithm, the choice of boundary conditions may not be physiological realistic, but are chosen from the literature [2, 3]. Simulation results for this branching model is shown in Figure 6.

Our algorithm again shows very good scalability to this complicated model; see Figure 7. Although there is a mild growth of GMRES iterations, the parallel speedup is nearly linear as we increase the number of processors. As for the overlapping additive Schwarz preconditioner, the overlap parameters δ is significant to the convergence of the linear system. In Table 2, we show the results of various choices of δ on different meshes and number of processors. By increasing the size of overlapping δ, the average number of GMRES iterations decreases. However, smaller overlapping sizes produce better timing results. It is always a trade off to choose the best δ. Large δ corresponds to a better preconditioner and fewer iterations. But large δ requires more communications and more time in subdomain solve, which may cost more in the total compute time.

5. Conclusion

In this paper, we introduced and studied an ALE based framework for fully coupled fluid-structure interaction problems for the simulations of blood flows in three-dimensional compliant arteries, and developed a parallel domain decomposition algorithm with an overlapping Schwarz preconditioner for solving the corresponding monolithically coupled, nonlinear system. We demonstrated that the Newton-Krylov-Schwarz algorithm allows us to simulate blood flows in compliant arteries both accurately and efficiently. In particular, the algorithm shows a great deal of robustness with respect to the complicated patient-specific geometries, large meshes and large number of processors. In the future, we plan to further develop this class of algorithms to include multilevel capabilities.

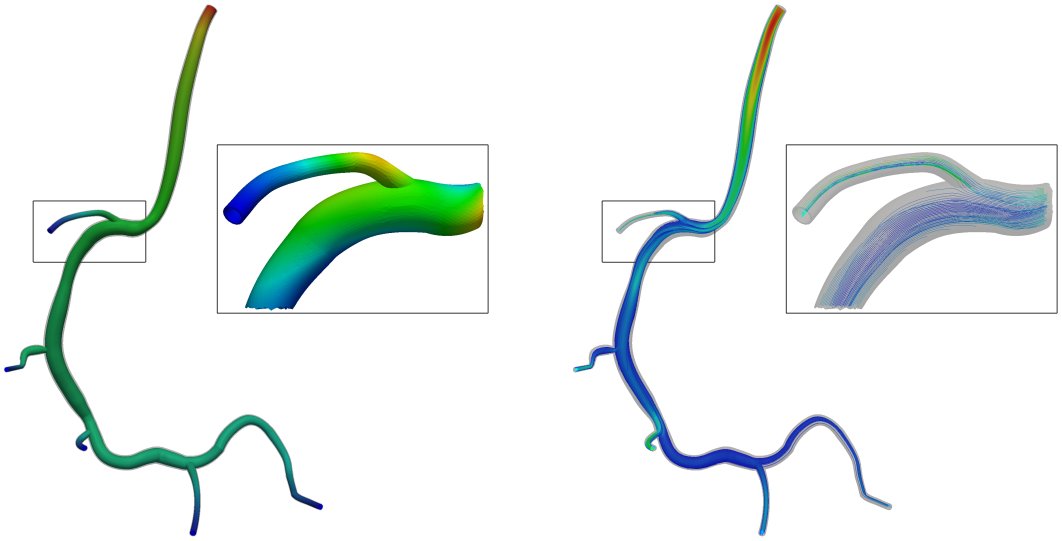

Figure 6: Results of a simulation on a branching geometry. In the large images, the fluid shaded by pressure is shown on the left, and the fluid velocity colored in its magnitude is shown on the right. The structure is shown in a solid shade in both images. In the inset images, the structure shaded by norm of the displacement is shown on the left, and the fluid streamlines colored by vorticity is shown on the right. Both insets representing a magnification of the marked portion.

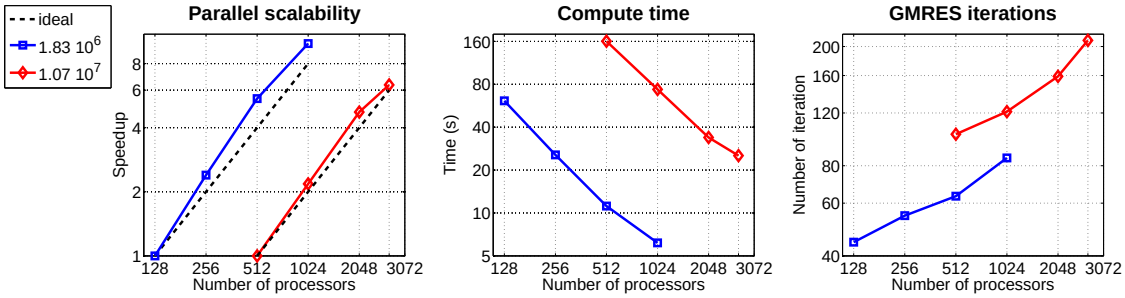

Figure 7: Parallel speedup, average compute time per time step, and average GMRES iterations per Newton iteration for the complex branching problem with increasing number of processors. The number of unknowns of each problem is listed in the legend.

unknowns	np	Newton			GMRES			time		
		δ=1	2	3	δ=1	2	3	δ=1	2	3
$1.83 \cdot 10^6$	256	2.0	2.0	2.0	54.50	47.45	42.85	25.58	29.85	33.03
	512	2.0	2.0	2.0	63.30	55.80	51.60	11.89	13.06	16.05
	1024	2.0	2.0	2.0	84.95	71.65	65.05	6.16	6.61	9.51
$1.07 \cdot 10^7$	512	2.0	2.0	2.0	101.90	74.15	64.50	160.50	197.05	258.04
	1024	2.0	2.0	2.0	121.20	96.90	88.20	73.66	94.40	140.72
	2048	2.0	2.0	2.0	159.00	118.80	102.50	33.89	38.19	54.88

Table 2: The effect of various choices of the overlapping parameter δ on different mesh sizes and number of processors. "np" denotes the number of processors. "Newton" denotes the average Newton iteration per time step. "GMRES" denotes the average GMRES iterations per Newton step. "time" refers to the average compute time, in seconds, per time step.

6. Acknowledgments

Special thanks to Professor Kendall Hunter and Professor Robin Shandas for their helpful discussions and acquiring clinical data for our model. Thanks also to the PETSc team of Argonne National Laboratory for their help and technical support on using the PETSc library.

References

[1] S. Balay, K. Buschelman, V. Eijkhout, W. Gropp, D. Kaushik, M. Knepley, L. Curfman McInnes, B. Smith, and H. Zhang. PETSc User Manual. Technical report, Argonne National Laboratory, 2010.

[2] A. T. Barker and X.-C. Cai. Scalable parallel methods for monolithic coupling in fluid-structure interaction with application to blood flow modeling. *J. Comput. Phys.*, 229:642–659, 2010.

[3] A. T. Barker and X.-C. Cai. Two-level Newton and hybrid Schwarz preconditioners for fluid-structure interation. *SIAM J. Sci. Comput.*, 32:2395–2417, 2010.

[4] Y. Bazilevs, V. M. Calo, T. J. R. Hughes, and Y. Zhang. Isogeometric fluid-structure interaction: theory, algorithms, and computations. *Comput. Mech.*, 43:3–37, 2008.

[5] X.-C. Cai and M. Sarkis. A restricted additive Schwarz preconditioner for general sparse linear systems. *SIAM J. Sci. Comput.*, 21:792–797, 1999.

[6] P. Causin, J. F. Gerbeau, and F. Nobile. Added-mass effect in the design of partitioned algorithms for fluid-structure problems. *Comput. Methods Appl. Mech. Engrg.*, 194:4506–4627, 2005.

[7] J. R. Cebral, M. A. Castro, J. E. Burgess, R. S. Pergolizzi, M. J. Sheridan, and C. M. Putman. Characterization of cerabral aneurysms for assessing risk of rupture by using patient-specific computational hemodynamics model. *AJNR Am J Neuroradial*, 26:2550–2559, 2005.

[8] P. Crosetto, P. Raymond, S. Deparis, D. Kontaxakis, N. Stergiopulos, and A. Quarteroni. Fluid structure interaction simulations of physiological blood flow in the aorta. *Computers and Fluids*, 43:46–57, 2011.

[9] S. Deparis, M. Discacciati, G. Fourestey, and A. Quarteroni. Fluid-structure algorithms based on Steklov-Poincaré operators. *Comput. Methods Appl. Mech. Engrg.*, 195:5797–5812, 2006.

[10] S. C. Eisenstat and H. F. Walker. Choosing the forcing terms in an inexact Newton method. *SIAM J. Sci. Comput.*, 17:16–32, 1996.

[11] M. A. Fernandez and M. Moubachir. A Newton method using exact Jacobians for solving fluid-structure coupling. *Comput. Struct.*, 83:127–142, 2005.

[12] C. A. Figueroa, I. E Vignon-Clementel, K. E. Jansen, T. J. R. Hughes, and C. A. Taylor. A coupled momentum method for modeling blood flow in three-dimensional deformable arteries. *Comput. Methods Mech. Engrg.*, 195:5685–5706, 2006.

[13] L. Formaggia, J. F. Gerbeau, F. Nobile, and A. Quarteroni. On the coupling of 3D and 1D Navier-Stokes equations for flow problems in compliant vessels. *Comput. Methods Appl. Mech. Engrg.*, 191:561–582, 2001.

[14] J. F. Gerbeau and M. Vidrascu. A quasi-Newton algorithm based on a reduced model for fluid structure problems in blood flows. *M2AN Math. Model. Numer. Anal.*, 37:663–680, 2003.

[15] M. Heil. An efficient solver for the fully-coupled solution of large-displacement fluid-structure interaction problem. *Comput. Methods Appl. Mech. Engrg.*, 193:1–23, 2004.

[16] T. J. R. Hughes, W. K. Liu, and T. K. Zimmermann. Lagrangian-Eulerican finite element formulation for incompressible viscous flows. *Comput. Methods Mech. Engrg.*, 29:329–349, 1981.

[17] F. Nobile. *Numerical Approximation of Fluid-structure Interatction Problems with Application to Haemodynamics*. PhD thesis, Ecole Polytechnique Federale de Lausanne, Lausanne, Switzerland, 2001.

[18] K. Takizawa, J. Christopher, T. E. Tezduyar, and S. Sathe. Space-time finite element computation of arterial fluid-structure interactions with patient-specific data. *Int. J. Numer. Meth. Fluids*, 26:101–116, 2010.

[19] C. A. Taylor and M. T. Draney. Experimental and computational methods in cardiovascular fluid mechanics. *Ann. Rev. Fluid Mech.*, 36:197–231, 2004.

[20] C. A. Taylor, T. J. R. Hughes, and C. K. Zarins. Finite element modeling of blood flow in arteries. *Comput. Methods Mech. Engrg.*, 158:155–196, 1998.

[21] T. E. Tezduyar, S. Sathe, T. Cragin, B. Nanna, B. S. Conklin, J. Pausewang, and M. Schwaab. Modelling of fluid-structure interactions with the space-time finite elements: Arterial fluid mechanics. *Int. J. Numer. Meth. Fluids*, 54:901–922, 2007.

[22] T. E. Tezduyar, S. Sathe, and K. Stein. Solution techniques for the fully discretized equations in computation of fluid-structure interactions with the space-time formulations. *Comput. Methods Mech. Engrg.*, 195:5743–5753, 2006.

[23] C. H. Whiting. *Stabilized Finite Element Methods for Fluid Dynamics Using a Hierarchical Basis*. PhD thesis, Rensselaer Polytechnic Institute, Troy, New York, 1999.

[24] C. H. Whiting and K. E. Jansen. A stabiliezed finite element method for the incompressible Navier-Stokes equations using a hierarchical basis. *Int. J. Numer. Meth. Fluids*, 35:93–116, 2001.

[25] Y. Wu and X.-C. Cai. A parallel two-level method for simulating blood flows in branching arteries with the resistive boundary condition. *Computers and Fluids*, 45:92–102, 2011.